

Heavy Quark Thermalization in Classical Lattice Gauge Theory: Lessons for Strongly-Coupled QCD

Mikko Laine^a, Guy D. Moore^{a,b}, Owe Philipsen^c, Marcus Tassler^c

^a*Faculty of Physics, University of Bielefeld, D-33501 Bielefeld, Germany*

^b*Department of Physics, McGill University, Montréal, QC H3A 2T8, Canada*

^c*Institute for Theoretical Physics, University of Münster, D-48149 Münster, Germany*

Abstract

Thermalization of a heavy quark near rest is controlled by the correlator of two electric fields along a temporal Wilson line. We address this correlator within real-time, classical lattice Yang-Mills theory, and elaborate on the analogies that exist with the dynamics of hot QCD. In the weak-coupling limit, it can be shown analytically that the dynamics on the two sides are closely related to each other. For intermediate couplings, we carry out non-perturbative simulations within the classical theory, showing that the leading term in the weak-coupling expansion significantly *underestimates* the heavy quark thermalization rate. Our analytic and numerical results also yield a general understanding concerning the overall shape of the spectral function corresponding to the electric field correlator, which may be helpful in subsequent efforts to reconstruct it from Euclidean lattice Monte Carlo simulations.

April 2009

1. Introduction

The real-time dynamics of heavy ion collisions is governed by QCD at relatively large coupling, which remains poorly understood despite significant theoretical efforts. While in principle both the weak-coupling expansion and lattice QCD provide systematically improvable schemes for the calculation of any physical quantity, including unequal-time correlation functions ($\Delta t \gg 1/T$) at a finite temperature T ($T \gtrsim 200$ MeV), both are in practice faced with serious limitations, related to the convergence of the weak-coupling expansion and to the need to carry out analytic continuation, respectively. Therefore many current attempts to describe the real-time dynamics of QCD at realistic temperatures rely on models. For instance, for heavy quark thermalization and diffusion, the main topics of the present paper, a relatively successful model treatment can be obtained by incorporating bound states as dynamical degrees of freedom into the description of an otherwise partonic medium [1]. Unfortunately, such models need typically to be tuned to the particular observable in question, rather than having a universal character, and also do not allow for a systematic improvement.

As an alternative to models, much recent literature has focused on *analogue theories*, by which we mean well-defined frameworks which are sufficiently close to QCD that most interesting QCD measurables have equivalents in the analogue, but which are nevertheless more amenable to calculation. Two such frameworks have been especially widely used: QCD truncated to the first non-trivial order in the weak-coupling expansion (see, e.g., ref. [2]), and $\mathcal{N}=4$ Super-Yang-Mills theory in the limit of an infinite number of colors and a large 't Hooft coupling (see, e.g., refs. [3, 4]).

QCD truncated to the first non-trivial order in the weak-coupling series is the starting point of a systematic expansion, and thus arguably the most similar analogue theory, guaranteed to be correct in the limit of a high temperature. The problem is that in the present setting it is technically extremely hard to work out subsequent terms in the weak-coupling series, given that extensive resummations are needed for dynamical quantities evolving over long time scales, and that in general several terms in the expansion would be needed, in order to obtain any kind of convergence. In fact, even though five subleading orders are available for thermodynamic (i.e. equal-time) quantities such as the pressure [5], convergence remains debatable [6]; in the dynamical case at most the first non-trivial order has been reached so far [7, 8, 9, 10], and the results certainly display very large $\mathcal{O}(g)$ corrections. This appears to indicate that the weak-coupling expansion is *not* well behaved except at very high temperatures, casting doubts on the physical relevance of truncated results in the realistic temperature range.

Super-Yang-Mills theory (SYM) resembles QCD in that it is a gauge theory with matter. However it contains many more matter multiplets than ordinary QCD, and in a different representation of the gauge group, which makes the matching between the theories ambigu-

ous [11]. Furthermore, computations on the SYM side are simple (using the famous AdS/CFT correspondence [12]) only in the limit of an infinite coupling, whereas the interesting regime is probably intermediate coupling.

In this paper we argue in favor of another analogue theory for the real-time dynamics of QCD: classical Yang-Mills theory regulated on a spatial lattice. This theory was developed by Kogut and Susskind [13] and has been used extensively to study the rate of Chern-Simons number diffusion in Yang-Mills theory [14], as well as (partly) out-of-equilibrium phenomena such as plasma instabilities [15], the dynamics of electroweak symmetry breaking [16], and inflationary preheating [17]. Recently, it was also applied for estimating the imaginary part of the real-time heavy-quark potential in QCD [18], and analogous methods were used for studying jet energy loss and transverse broadening in a hot non-Abelian plasma [19]. In this approach the infrared (IR) behavior of QCD is approximated by introducing semiclassical fields, while in the ultraviolet (UV) the quantum mechanical “cutoff” on thermal effects from short distances is replaced with a lattice cutoff. Formally, the classical limit corresponds to taking $\hbar \rightarrow 0$, which is a non-trivial limit at non-zero temperatures [20, 21], and non-singular in the presence of the lattice cutoff.

In this paper we use this framework to study one of the simplest gauge-invariant observables, the correlator of two electric fields along a Wilson line,

$$\kappa(\omega) \equiv \frac{\frac{1}{3} \sum_{i=1}^3 \int dt e^{i\omega t} \text{Tr} \langle U(-\infty - i\beta, t) gE_i(t, \mathbf{0}) U(t, 0) gE_i(0, \mathbf{0}) U(0, -\infty) \rangle}{\text{Tr} \langle U(-\infty - i\beta, t) U(t, 0) U(0, -\infty) \rangle}, \quad (1.1)$$

where $\beta \equiv 1/T$; $gE_i \equiv i[D_0, D_i]$ is the color-electric field; $U(t_b, t_a)$ represents a temporal Wilson line from t_a to t_b at a fixed spatial location $\mathbf{x} = \mathbf{0}$; and the trace is over the fundamental representation. The denominator removes any regularization issues associated with the Wilson lines themselves. The zero-frequency limit $\kappa(0)$ of this correlator is the momentum diffusion coefficient of a heavy quark [4, 22], and the combination $\eta_D = \kappa(0)/2M_{\text{kin}}T$ emerging from linear response relations, with M_{kin} denoting the so-called kinetic mass of the heavy quark, determines the heavy quark thermalization rate [2, 22, 23].

Our goals and the organization of the paper are as follows. In Sec. 2, we describe the basic ideas behind classical lattice gauge theory as a tool for studying real-time quantities in QCD. In Sec. 3, we focus more precisely on the observable in Eq. (1.1), and use the weak-coupling regime to study how close the analogy between the two theories really is. The limitations of classical lattice gauge theory as a model for QCD are also illustrated, by studying the unphysical “strong-coupling” limit of the lattice-regulated theory. In Sec. 4, we discuss the results we obtain at intermediate couplings, where the weak-coupling expansion fails yet classical lattice gauge theory still captures the correct infrared dynamics that causes the failure. Some discussion and conclusions can be found in Sec. 5, while two appendices contain details related to the weak and strong-coupling regime on the classical lattice, respectively.

2. Classical Lattice Theory: Basic Idea

At a temperature far above the confinement scale, such that the effective gauge coupling g is small, QCD (whether pure-gluon or with dynamical quarks) possesses three different parametric length scales (\equiv inverse momentum scales):

- the length scale $(\pi T)^{-1}$, where most of the energy resides;
- the “color-electric” length scale $(gT)^{-1}$, where plasma screening effects become important and perturbation theory needs to be resummed [24]; and
- the “color-magnetic” length scale $(g^2T/\pi)^{-1}$, where interactions become genuinely non-perturbative. The longest spatial correlation lengths of gauge invariant operators are on this scale [25].

Different real-time correlation functions and physical properties of QCD are sensitive to different scales. For instance, the Chern-Simons diffusion rate is sensitive dominantly to the momentum scale g^2T/π ; it depends on the other scales only in that they change the dynamics on this scale. Scattering, radiation and energy loss are sensitive mostly to the scale gT . This scale therefore captures much of the physics of current interest in heavy ion collisions, such as jet quenching and heavy quark thermalization. Shear viscosity, on the other hand, is principally sensitive to the scale πT , since most of the energy and momentum reside there.

Since for the momentum scales $p \sim gT, g^2T/\pi$ the loop expansion parameter related to bosonic fields, $\epsilon \sim g^2\hbar/(e^{\beta\hbar p} - 1)$, can parametrically be replaced with its classical limit, g^2T/p , it can be argued [26] and shown formally [20] that the physics at the scales $gT, g^2T/\pi$ is described by classical statistical field theory. Quantum mechanics is only relevant at the scale πT , where its role is to ensure that thermal excitations on short scales are suppressed. The idea of the lattice analogue theory is to suppress thermal excitations on short scales instead by imposing a spatial lattice cutoff. The resulting theory is a classical field theory on all scales. At weak coupling it remains a three-scale theory, with:

- the length scale a , where most of the energy resides;
- the color-electric length scale $(g^2T/a)^{-1/2} \sim a\beta_L^{1/2}$, where plasma screening effects become important and perturbation theory needs to be resummed [27, 28]; and
- the length scale $(g^2T/\pi)^{-1} \sim a\beta_L$, where interactions become non-perturbative. The longest spatial correlation lengths of gauge invariant operators are on this scale.

Here we have introduced the “lattice coupling”, $\beta_L \equiv 2N_c/g^2Ta$, which controls whether interactions are perturbative at the lattice spacing scale.

Physics at the scale a is definitely different from physics of the quantum theory at the scale $(\pi T)^{-1}$. In particular, lattice discretization breaks translational invariance so there is no

conserved momentum. This changes hydrodynamic behavior in an essential way, so one should not try to study shear viscosity with the classical theory. However, the more infrared scales, describing “collective phenomena”, are only changed to the extent that the loop effects they feel from the hard momenta, associated with the expansion parameter $\epsilon \sim g^2 T/p \sim g^2 T a$, differ from the corresponding quantum loop effects, with $\epsilon \sim g^2/\pi$.

For equal-time quantities, these radiative effects turn out to be rotationally invariant and of exactly the same form as in the continuum quantum theory. They are simply a Debye mass parameter for the A_0 field, of magnitude [29]

$$m_{\text{D,cont}}^2 = \frac{2N_c + N_f}{6} g^2 T^2, \quad (2.1)$$

$$m_{\text{D,latt}}^2 = \frac{2N_c \Sigma}{4\pi} \frac{g^2 T}{a}, \quad \Sigma = 3.175911536 \dots \quad (2.2)$$

Equating these gives a concrete way of relating the lattice spacing a and the temperature T , $a \simeq 3\Sigma N_c/\pi T(2N_c + N_f)$. [Note that the $p \sim 1/a$ lattice modes are playing the role both of ultraviolet gluonic degrees of freedom (the $2N_c$) as well as of quark fields (the N_f); infrared quarks can be neglected because at low frequencies the Fermi-Dirac distribution function is much smaller than the Bose-Einstein one.] At the dynamical level, however, radiative effects are no longer rotationally invariant [27, 28], which means that any “matching” between the lattice scale a and the temperature T is ambiguous, and only makes sense in order-of-magnitude. We return to this issue in more detail in the next section.

Considering finally the color-magnetic scale, it remains the same, $g^2 T/\pi$, in both theories. In other words, the precise form of the ultraviolet regulator is invisible to physics at the largest distances. At the same time, the dynamics on the scale $g^2 T/\pi$ is non-perturbative [25], but can relatively easily be simulated numerically through the classical description.

Consider now the “weak-coupling regime” where the three scales are widely separated, and an observable dominantly determined by the scale gT . Its exact value is given by the leading order result modified by relative corrections suppressed by $\epsilon \sim g^2 T/p$. While corrections from the hard scale $p \sim \pi T$ may remain controllably small down to low temperatures (cf., e.g., ref. [30]), experience with many observables such as the plasmon frequency [7], the heavy quark diffusion coefficient [8], the light quark dispersion relation [9], the jet quenching parameter \hat{q} [10], or the Debye screening length [31], has shown that radiative corrections from the scale $p \sim gT$ itself can be very large (even if parametrically perturbative). The challenge would therefore be to sum the corrections from the scales $p \sim gT, g^2 T/\pi$ to all orders.

The key property of the classical lattice theory is that it is amenable to a numerical simulation, and therefore indeed allows for all-orders resummations of the type mentioned to be carried out in practice. Should the large corrections come from the scale $p \sim gT$ in the quantum theory, they are somewhat distorted in the classical lattice gauge theory, but

the results are still representative of the qualitative behavior. The contact to the quantum theory is only lost in the “strong-coupling regime” where $\beta_L \lesssim 1$; then all three scales are of the same order and the physics differs essentially from the quantum theory.

3. Classical Lattice Theory: Electric Field Correlator

In the previous section we argued on general grounds that classical lattice gauge theory and thermal QCD have qualitative and, in the very infrared, even quantitative similarities. We now want to demonstrate this explicitly for the case of heavy quark thermalization.

Let us start by recalling the reason for why the zero-frequency limit of Eq. (1.1) describes heavy quark momentum diffusion [4] and consequently thermalization [2, 22, 23] (on the formal level, the correspondence can be derived by making use of the heavy quark effective field theory [22]). In a classical framework, it is quite easy to see why this is the case. Intuitively, the field gE_i exerts a Lorentz force on a charge carrier, and $\kappa \equiv \kappa(0)$ is the total correlation of that force with previous and future forces. The force changes the momentum of the heavy quarks. The classical lattice theory does not contain any heavy quarks, but we can still evaluate the force–force correlation function to see what momentum diffusion a heavy quark would feel.

We discretize classical lattice gauge theory as in ref. [14] and sample its thermal ensemble using the algorithm of ref. [32] (we recommend ref. [32] for a more detailed description of the procedure). The classical simulation is generally carried out in a gauge where the temporal links equal unity; thereby all the Wilson lines disappear from Eq. (1.1), and we only need to correlate the electric fields. For a comparison we have also carried out some simulations with the “improved” lattice action of ref. [33], which provides a dispersion relation conforming more tightly to the continuum one, though it also differs significantly for $p \sim 1/a$. On the quantum theory side operator ordering plays a role; in the following we assume symmetric ordering (for details, see ref. [22]), whereby the quantum correlator has the same symmetries as the classical one; this can be obtained by $\kappa(\omega) \rightarrow [\kappa(\omega) + \kappa(-\omega)]/2$ from the case literally shown in Eq. (1.1).

To start with we compare the theories at the free level. In the continuum theory,

$$\kappa_{\text{cont}}(\omega) = [1 + 2n_{\text{B}}(\omega)] \frac{g^2 C_{\text{F}} \omega^3}{6\pi}, \quad (3.1)$$

$$\kappa_{\text{cont}}(t) = g^2 C_{\text{F}} T^4 \pi^2 \left[\frac{\cosh^2(\pi t T)}{\sinh^4(\pi t T)} - \frac{1}{3 \sinh^2(\pi t T)} \right], \quad (3.2)$$

where n_{B} is the Bose-Einstein distribution function. The vacuum behavior of $\kappa_{\text{cont}}(t)$ reads

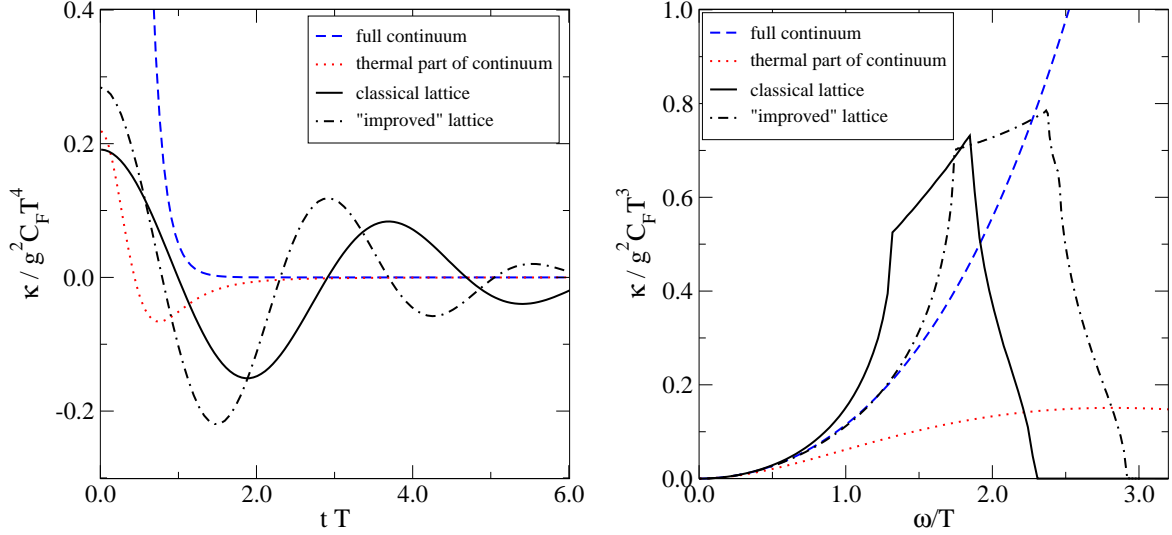


Figure 1: The correlation function $\kappa(t)$ (left) and its Fourier transform $\kappa(\omega)$ (right) in the quantum continuum and classical lattice theories, at leading order (free level). To relate the theories, we convert the lattice spacing a to the inverse temperature $1/T$ by equating Debye lengths for the pure-gluon theory ($N_f = 0$), whereby $a = 3\Sigma/2\pi T$ (cf. discussion below Eq. (2.2)).

$g^2 C_F T^4 \pi^2 / (\pi t T)^4$. In the classical lattice theory, on the other hand,

$$\kappa_{\text{latt}}(\omega) = \frac{2\pi g^2 C_F T}{3} \int_{-\pi/a}^{\pi/a} \frac{d^3 \mathbf{p}}{(2\pi)^3} \left[\delta(\tilde{p} - \omega) + \delta(\tilde{p} + \omega) \right], \quad (3.3)$$

$$\kappa_{\text{latt}}(t) = \frac{2g^2 C_F T}{3} \int_{-\pi/a}^{\pi/a} \frac{d^3 \mathbf{p}}{(2\pi)^3} \cos(\tilde{p}t), \quad (3.4)$$

where $\tilde{p} \equiv \sqrt{\tilde{p}^2}$, $\tilde{p}^2 \equiv \sum_i \tilde{p}_i^2 \equiv \sum_i (\frac{2}{a} \sin \frac{ap_i}{2})^2$. The results are plotted¹ in Fig. 1. At first sight the lattice correlator and the vacuum-subtracted thermal correlator do *not* look alike: the main difference is in the large-time behavior, where the continuum correlator dies away but the lattice correlator displays decaying oscillations. The difference is explained when we look at the frequency-domain correlation functions. Here we see that the lattice correlator has cusps while the continuum correlator is smooth. The cusps are van Hove singularities which arise because the lattice excitations follow a modified dispersion relation²,

$$\omega_{\text{latt}}^2(p) = \tilde{p}^2, \quad (3.5)$$

which has vanishing slope at the corners of the Brillouin zone, $\mathbf{p} = (n_1, n_2, n_3)\pi/a$, leading to cusps in the density of states at $\omega_{\text{latt}}^2 = (4, 8, 12)/a^2$. These van Hove singularities are

¹The “thermal part” is the difference of the full and vacuum parts, and it is this difference which is relevant for heavy quark thermalization.

²The dispersion relation for the “improved” action is more complicated, see Eqs. (66,67) of ref. [33] [Eqs. (63,64) in the journal version]; the overall sign is wrong in the latter equation.

well understood and have little impact on the small- ω behavior which is actually of interest. In the small-frequency region $\omega \ll T$ the theories do agree completely. In other words, the rather dramatic difference in the time-domain behavior shown on the left in Fig. 1 arises because $\kappa(t)$ is principally sensitive to the T or $1/a$ scale, where the theories are different; when we look at the frequency domain, the large frequency behaviors are very different as expected, but the low frequency parts agree. However, at the free level, the intercept $\kappa(0)$ is zero on both sides, so we need to consider interactions.

The leading non-zero value for $\kappa(0)$ turns out to involve a logarithm of the scales πT and gT . Considering the logarithm from the IR side, its origin lies in the fact that the electric gauge field self-energy gets an imaginary part for $|\omega| < |\mathbf{p}| \sim gT$, corresponding to the phenomenon of Landau damping (it also gets a real part, corresponding to Debye screening). The result for κ is related to the cut of the electric field propagator, and can be written as

$$\begin{aligned} \kappa_{\text{cont}} &\simeq \frac{8\pi g^4 C_F N_c}{3} \int_{p \ll T} \frac{d^3 \mathbf{p}}{(2\pi)^3} \frac{p^2}{(p^2 + m_D^2)^2} \int \frac{d^3 \mathbf{q}}{(2\pi)^3} \delta((p-q)^2 - q^2) q n_B(q) [1 + n_B(q)] \\ &\simeq \frac{g^2 C_F T m_D^2}{6\pi} \left(\ln \frac{T}{m_D} + \dots \right), \end{aligned} \quad (3.6)$$

where $C_F \equiv (N_c^2 - 1)/2N_c$ is the Casimir of the heavy quark representation. Here we omitted for notational simplicity quarks, and carried out the integral $2g^2 N_c \int_{\mathbf{q}} n_B(q) [1 + n_B(q)] = T m_D^2$. The full computation and the result for the coefficient accompanying the logarithm can be found in ref. [2].

Consider then the classical lattice theory side. Restricting again to the leading logarithmic order, the only modifications needed are as follows:

- The statistical functions $n_B(q)$ and $1 + n_B(q)$ are replaced by their classical limits T/q ;
- Dispersion relations and propagators use \tilde{p}_i, \tilde{q}_i in place of p_i, q_i .

Furthermore, at the order considered, the diagram is dominated by small exchange momentum p , and we can approximate the argument of the δ -function as $(\widetilde{p-q})^2 - \tilde{q}^2 = 2\tilde{\mathbf{p}} \cdot \hat{\mathbf{q}} + \mathcal{O}(p_i^2)$, where $\hat{q}_i \equiv \frac{1}{a} \sin(aq_i)$. Thereby the lattice version of Eq. (3.6) becomes

$$\begin{aligned} \kappa_{\text{latt}} &\simeq \frac{4\pi g^4 T^2 C_F N_c}{3} \int_{-\pi/a}^{\pi/a} \frac{d^3 \mathbf{p}}{(2\pi)^3} \frac{\tilde{p}^2}{(\tilde{p}^2 + m_{D,\text{latt}}^2)^2} \int_{-\pi/a}^{\pi/a} \frac{d^3 \mathbf{q}}{(2\pi)^3} \frac{\delta(\tilde{\mathbf{p}} \cdot \hat{\mathbf{q}})}{\tilde{q}} \\ &\simeq \frac{g^4 T^2 C_F N_c}{3\pi} \int_{-\pi/a}^{\pi/a} \frac{d^3 \mathbf{q}}{(2\pi)^3} \frac{1}{\sqrt{\tilde{q}^2 \hat{q}^2}} \times \left(\ln \frac{1}{am_{D,\text{latt}}} + \dots \right). \end{aligned} \quad (3.7)$$

Here we made use of the fact that for $p \sim m_{D,\text{latt}} \ll 1/a$, \mathbf{p} can be viewed as a continuum variable, so one can carry out an angular integral to remove the δ -function. We calculate the constant accompanying the logarithm, denoted by ... in Eq. (3.7), in Appendix A, finding it to be $1.8313(2)$.

In Eqs. (2.1), (2.2), we saw the correspondence

$$m_{\text{D,cont}}^2 \leftrightarrow 2g^2 N_c T \frac{\Sigma}{4\pi a}, \quad (3.8)$$

where the defining expression for Σ reads

$$\frac{\Sigma}{4\pi a} \equiv \int_{-\pi/a}^{\pi/a} \frac{d^3 \mathbf{q}}{(2\pi)^3} \frac{1}{\tilde{q}^2}. \quad (3.9)$$

Comparing the coefficients of the logarithms in Eqs. (3.6), (3.7), on the other hand, suggests the correspondence

$$m_{\text{D,cont}}^2 \leftrightarrow 2g^2 N_c T \int_{-\pi/a}^{\pi/a} \frac{d^3 \mathbf{q}}{(2\pi)^3} \frac{1}{\sqrt{\tilde{q}^2 \hat{q}^2}}. \quad (3.10)$$

The difference between Eqs. (3.8), (3.10) is a manifestation of the ambiguity in the matching of the continuum and lattice theories that was mentioned in Sec. 2. More generally, noting that the dispersion relation in Eq. (3.5) gives a group velocity

$$|v_{\text{group}}(q)| \equiv \sqrt{\frac{\hat{q}^2}{\tilde{q}^2}}, \quad (3.11)$$

and defining

$$\frac{\Sigma_{v^n}}{4\pi a} \equiv \int_{-\pi/a}^{\pi/a} \frac{d^3 \mathbf{q}}{(2\pi)^3} \frac{|v_{\text{group}}(q)|^n}{\tilde{q}^2}, \quad (3.12)$$

we can write

$$\kappa_{\text{latt}} \approx \frac{g^2 C_F T m_{\text{D,latt}}^2}{6\pi} \frac{\Sigma_{v^{-1}}}{\Sigma} \times \left(\ln \frac{1}{am_{\text{D,latt}}} + 1.831 \right). \quad (3.13)$$

A similar correspondence was found in ref. [28] for a number of other quantities: scaling away $m_{\text{D,latt}}^2$, the Debye screening length involves $\Sigma_{v^0} = \Sigma$; infrared magnetic damping involves Σ_{v^1} ; and the plasmon oscillation frequency involves Σ_{v^2} .³ What we have shown is that Coulombic scattering (electric damping) involves $\Sigma_{v^{-1}}$. The numerical value of each Σ_{v^n} is given in Table 1. The fact that they do not coincide means that there is some ambiguity in how to relate the lattice and continuum theories. Nevertheless, the general structures of the answers in Eqs. (3.6), (3.7), including the existence of logarithms, are the same, whereby we can conclude that the dynamics of the two theories indeed bear a strong *qualitative* resemblance to each other.

³Each v dependence arises from simple physics. κ_{latt} is the mean squared momentum a charged particle absorbs due to Coulomb interactions with passing excitations. An excitation with velocity v has a flux factor suppressed by v but it interacts for $1/v$ times as long, giving a force-squared enhanced by v^{-2} ; hence κ_{latt} involves v^{-1} . Magnetic damping is similar but it involves magnetic forces, which are suppressed by v relative to Coulombic forces. Therefore the mean squared momentum exchange scales as v^0 , leaving only the flux factor v^1 . Plasma oscillations involve the mean squared current generated by an oscillating electric field; the current is proportional to v of the charges, so $\omega_{\text{pl}}^2 \sim v^2$. Debye screening is a thermodynamic property so it shows no scaling with group velocity.

	“standard” [14]	“improved” [33]
Σ_{v^2}	1.6222746498	1.78576519
Σ_{v^1}	2.1498783949	2.13792379
Σ_{v^0}	3.1759115356	2.783189232
$\Sigma_{v^{-1}}$	5.5079614967	4.1679252

Table 1: Values of Σ_{v^n} for the standard and “improved” lattice actions. The spread of values is a measure of how different the structure of the lattice Hard Thermal Loops is from the continuum ones.

The discussion so far has assumed that we are in the weak-coupling regime, i.e. that β_L is large. If β_L decreases so much that all three momentum scales are of the same order of magnitude, then the behavior of κ_{latt} changes significantly. Scaling κ_{latt} dimensionless by multiplying with a^3 , and making use of the definition of β_L , the weak-coupling behavior in Eq. (3.13) corresponds to

$$a^3 \kappa_{\text{latt}} \stackrel{\beta_L \gg 1}{\sim} \frac{1}{\beta_L^2} \ln \beta_L, \quad (3.14)$$

while at small β_L we find, through the arguments in Appendix B, the behavior

$$a^3 \kappa_{\text{latt}} \stackrel{\beta_L \ll 1}{\sim} \frac{1}{\beta_L^{5/2}}. \quad (3.15)$$

The physics behind this functional form is very specific to the nature of the lattice variables, however, so we do not expect any analogy with the continuum quantum theory in the latter regime, and refrain from a further discussion here.

4. Numerical Results

In the previous section we have verified that, at weak coupling, the electric field correlator in classical lattice gauge theory behaves quite similarly to physical QCD: if we fix the lattice spacing a by equating the Debye screening lengths, the leading-logarithmic κ of the classical lattice theory is larger than that in the quantum continuum theory by a factor $\Sigma_{v^{-1}}/\Sigma_{v^0} \sim 5/3$. We now proceed to larger values of the coupling (smaller β_L) with the help of numerical simulations. At relatively small coupling (large β_L), we can check how fast the weak-coupling regime is approached. At stronger coupling (intermediate $\beta_L \sim 1$), we can find out whether the leading-order weak-coupling result is reasonable even in order of magnitude, and whether it underestimates or overestimates the actual behavior. This then gives us some guidance for what to expect in QCD.

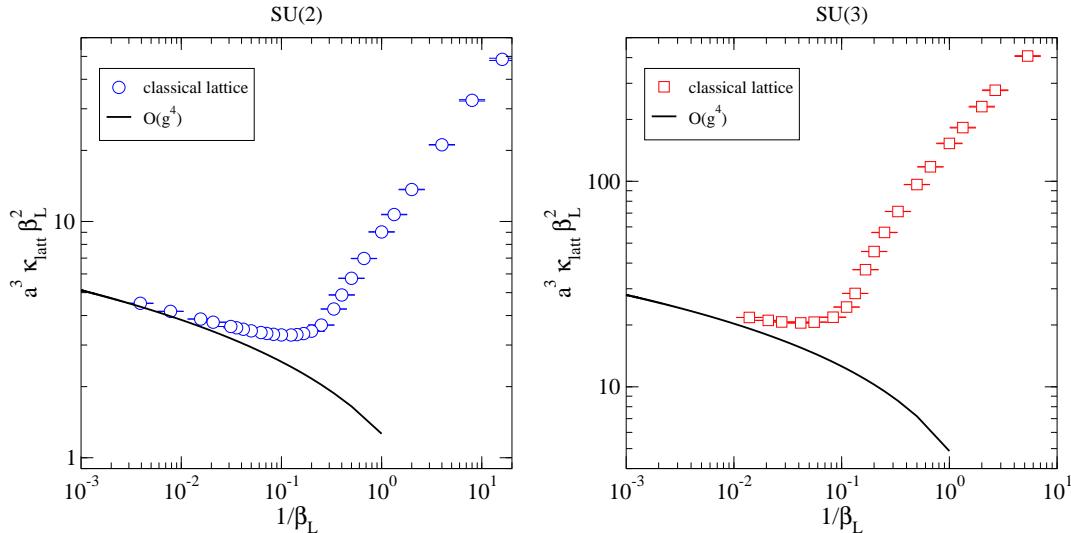


Figure 2: Numerical results for the intercept κ_{latt} (open symbols), compared with the weak-coupling prediction from Eq. (3.13) (line). The left plot is for SU(2), the right one for SU(3). Note that $1/\beta_L = g^2 T a / 2N_c$ scales like α_s , assuming the matching $a \sim 1/T$ (cf. discussion after Eq. (2.2)).

4.1. Intercept at $\omega \rightarrow 0$

Our numerical results for κ_{latt} , compared with the leading-order weak-coupling result, are shown in Fig. 2, both for SU(2) [included because a large β_L -range could be scanned with a modest numerical effort] and for SU(3).⁴ We note, first of all, that at large β_L , the results approach the analytic ones of Eq. (3.13). However, as soon as $\beta_L \lesssim 100$, the non-perturbative results deviate from the leading-order ones. The non-perturbative results are always *larger* than the perturbative estimate. For $\beta_L = 1 \dots 10$, a crossover takes place⁵ from one type of behavior to another. At $\beta_L \ll 1$, the results approach the behavior of Eq. (3.15). (We have not worked out the numerical prefactor for Eq. (3.15), and hence do not show the corresponding curves in Fig. 2.)

In order to make quantitative use of the numerical results, it is convenient to change the units of both axes. Recalling the definition of $m_{\text{D,latt}}^2$ from Eq. (2.2), we choose the variable $g^2 N_c T / m_{\text{D,latt}} = 2N_c (\pi / \Sigma \beta_L)^{1/2}$ as the x -coordinate; this quantity is the ratio of the $g^2 T$ to gT scales and is therefore the expansion parameter for perturbation theory at the scale gT . We also divide $a^3 \kappa_{\text{latt}}$ by the coefficient of the leading logarithm, $a^3 g^2 C_F T m_{\text{D,latt}}^2 / 6\pi = C_F N_c^3 \Sigma / 3\pi^2 \beta_L^2$. In these units, the lattice results have a direct counterpart in the continuum

⁴In the numerical implementation the theory is discretized in time as well as space, but with a much finer spacing, and our numerical results for κ_{latt} represent the limit of zero temporal spacing. We have also checked that our results contain no significant finite volume or non-zero ω artifacts.

⁵We have checked that there is no actual phase transition in the thermodynamics of the system.

theory. The weak-coupling regime is plotted in the new units in Fig. 3.

In the continuum theory, corrections of $\mathcal{O}(g^5)$ to κ_{cont} have recently been determined [8], and it is now interesting to compare the results. According to ref. [8],

$$\kappa_{\text{cont}} = \frac{g^2 C_F T m_{\text{D,cont}}^2}{6\pi} \left(\ln \frac{T}{m_{\text{D,cont}}} + C_{\text{cont}} + D_{\text{cont}} \frac{N_c g^2 T}{m_{\text{D,cont}}} + \dots \right), \quad (4.1)$$

with $D_{\text{cont}} = 0.7767$. The physics giving rise to D_{cont} involves only the length scale gT and should be reproduced on the lattice; however, it depends on the structure of the Hard Thermal Loops in an essential way, so the lattice value could differ by up to $\mathcal{O}(50\%)$ as discussed in the previous section. Still, this motivates a fit of the lattice data to the form

$$\kappa_{\text{latt}} = \frac{g^2 C_F T m_{\text{D,latt}}^2}{6\pi} \left(\frac{\Sigma_{v-1}}{\Sigma} \ln \frac{1}{am_{\text{D,latt}}} + C_{\text{latt}} + D_{\text{latt}} \frac{N_c g^2 T}{m_{\text{D,latt}}} + \dots \right), \quad (4.2)$$

where $C_{\text{latt}} = 1.831 \times \Sigma_{v-1}/\Sigma = 3.176$. The coefficient D_{latt} can confirm the sign and approximate magnitude of D_{cont} . It can also tell us about the next terms in the expansion, in particular whether the $\mathcal{O}(g^5)$ calculation is an underestimate or an overestimate of the real κ . Note, however, that the next term, of $\mathcal{O}(g^6)$, would receive contributions not only from the scale gT but also from the scale πT , so the relation between the lattice and continuum theories becomes less precise at this order.

Fig. 3 shows the (1-parameter) fit to the lattice data according to Eq. (4.2). The fit is very good out to $g^2 N_c T / m_{\text{D,latt}} \sim 1.5$. We extract the value $D_{\text{latt}} = 0.87(4)$, in surprisingly good agreement with $D_{\text{cont}} = 0.7767$; and we see that the same coefficient D_{latt} fits the SU(2) and SU(3) data, just as the continuum computation predicts. However, at larger couplings κ_{latt} rises *above* the fitted behavior, particularly for the group SU(3).

The above results no doubt depend on the details of the numerical implementation of the lattice theory and of the electric field operator. As a check on the robustness of our results, we re-compute them using the “improved” lattice action of ref. [33]. This action is tree-level improved so that the IR behavior naively coincides more tightly with the continuum, as shown for instance by the better IR behavior of the free-theory correlator $\kappa(\omega)$ in Fig. 1. However the UV behavior still has (different) anisotropic non-ultrarelativistic dispersion, so the Hard Thermal Loop effects are not those of the continuum (though they are somewhat closer, as reflected by the slightly narrower spread of the Σ_{v^n} values in Table 1). Therefore it is better to think of this implementation as “different” rather than truly “improved.”

Fig. 4 shows $\kappa(0)$ as a function of the lattice coupling for the “different”/“improved” lattice action for the group SU(2). While the lattice constants $C_{\text{latt}} = 2.5$ and $D_{\text{latt}} = 0.64$ (this time both are fitted) differ from the “standard” action values, the qualitative message is the same; at weak coupling the behavior appears to be well described by next-to-leading order perturbation theory, but at stronger coupling perturbation theory is an underestimate. But while for $\beta_L \gtrsim 1$ the two implementations give similar qualitative results, at extremely strong

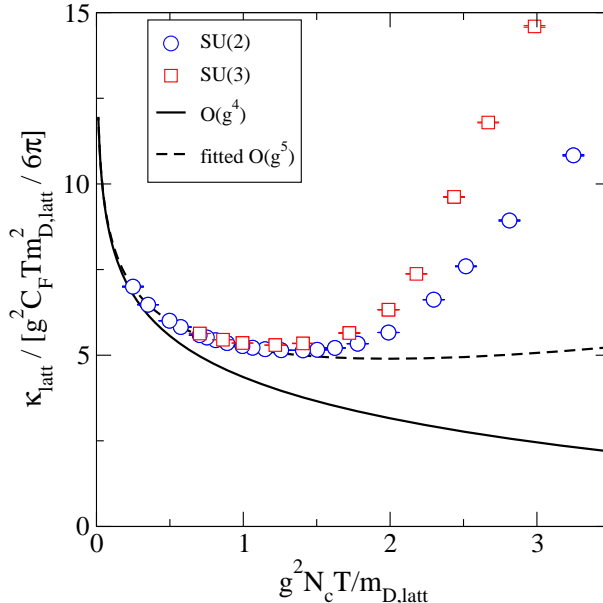


Figure 3: κ_{latt} , normalized to the leading-order perturbative behavior, expressed as a function of the expansion parameter $g^2 N_c T / m_{D,\text{latt}}$ related to corrections from the scale gT . At weak coupling, the SU(2) and SU(3) results agree and are well fit by the $\mathcal{O}(g^5)$ perturbative behavior. At stronger coupling, κ_{latt} rises above the perturbative fit, by a group dependent amount. Compared with Fig. 2, the horizontal axis is restricted to $1/\beta_L \leq 0.77$ for SU(2), $1/\beta_L \leq 0.34$ for SU(3).

coupling the behaviors are not even qualitatively the same. This reinforces our belief that the $\beta_L \lesssim 1$ behavior is a lattice artifact with no bearing on QCD.

We finally attempt a rough order-of-magnitude estimate for which β_L -range corresponds to the situation met in heavy ion collision experiments. Combining the matching from below Eq. (2.2) with the definition of β_L , we get

$$\beta_L \sim \frac{2N_c + N_f}{6\Sigma\alpha_s}. \quad (4.3)$$

The relevant value of α_s can in the present context probably best be approximated by taking it from the dimensionally reduced effective theory [34], to which the classical lattice gauge theory reduces in the case of equal-time observables. In this limit the coupling has been computed up to 2-loop level [30]; for $N_f = 3$ the values are $g^2 \sim 3\dots 2$ for $T/\Lambda_{\overline{\text{MS}}} \sim 1\dots 4$, corresponding to $\alpha_s = 0.24\dots 0.16$, and subsequently $\beta_L = 2\dots 3$. This corresponds to $g^2 N_c T / m_{D,\text{latt}} = 4\dots 3$.

Remarkably, in the range $\beta_L = 2\dots 3$, the numerical SU(3) values in Fig. 2 exceed the weak-coupling result by as much as an order of magnitude! Though these values of β_L are so small that the matching cannot be trusted on any kind of quantitative level, such a huge effect is still encouraging both from the experimental point of view [35], where the apparently very rapid thermalization of heavy quarks remains a mystery, as well as from the point of view of

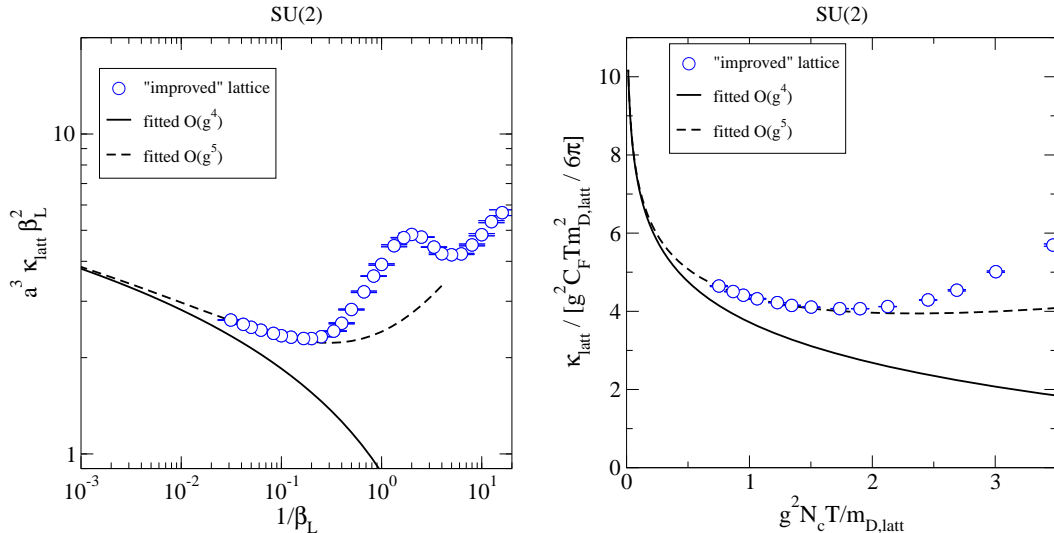


Figure 4: κ_{latt} using the “improved” lattice action. Left: the overall behavior in lattice units. Right: a magnification of the weak-coupling regime, normalized to the leading-order perturbative behavior. The weak-coupling behavior is in good qualitative accord with the standard action, but the strong coupling behavior is qualitatively different (cf. Figs. 2, 3).

following the suggestion of ref. [22] in order to measure κ_{cont} with Euclidean lattice Monte Carlo methods. Indeed, there may well be an exciting qualitative discovery to be made on the lattice.

4.2. General shape of the spectral function

On the point of lattice Monte Carlo simulations, ref. [22] argued that the Euclidean analogue of Eq. (1.1) leads to a correlator, denoted by $G_E(\tau)$, which has a non-trivial continuum limit and can be related to the intercept κ_{cont} through standard relations. Specifically, the task would be to invert the relation

$$G_E(\tau) = \int_0^\infty \frac{d\omega}{\pi} \kappa_{\text{cont}}(\omega) \frac{\cosh\left(\frac{\beta}{2} - \tau\right) \omega}{\cosh \frac{\beta\omega}{2}}. \quad (4.4)$$

It is a problem, though, that strictly speaking the relation in Eq. (4.4) is not invertible without further input. In practice, this means that a certain *Ansatz* (sometimes called a prior) is needed, which is then refined through the numerical data. For this reason, significant efforts have been devoted to analytic computations of spectral functions in the presence of a spatial lattice, in the limit of a high temperature, for cases such as the 2-point correlator of the vector current of heavy quarks [36].

We can now use our data, both perturbative as well as non-perturbative, to obtain an *Ansatz* for the spectral function $\kappa_{\text{cont}}(\omega)$. In Fig. 5, results are shown for the function

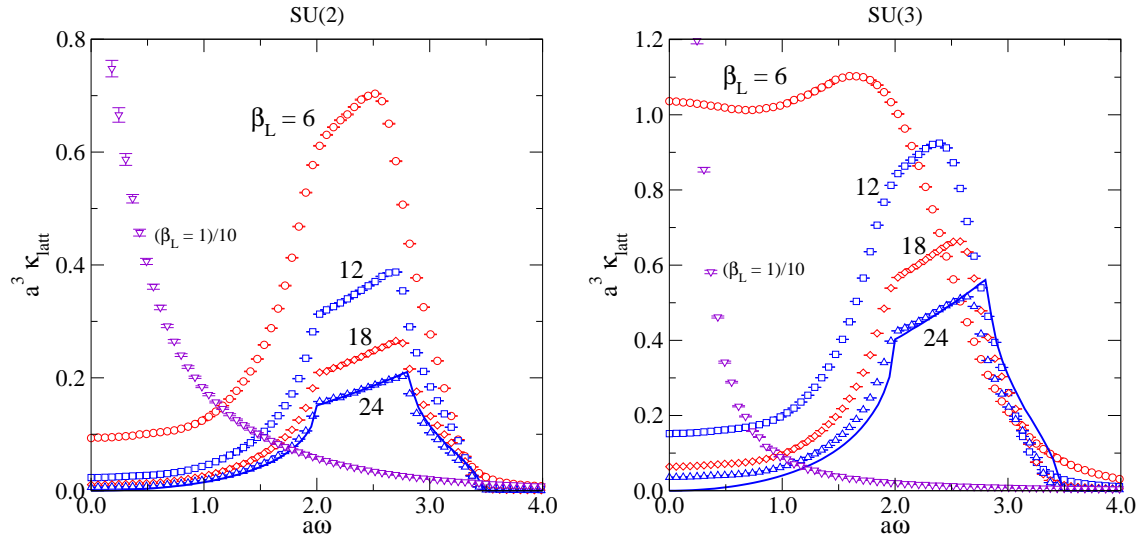


Figure 5: Numerical results for the function $a^3 \kappa_{\text{latt}}$ (open symbols), compared with the weak-coupling prediction from Eq. (3.3) for $\beta_L = 24$ (line). The left plot is for SU(2), the right one for SU(3). For the (unphysical) case $\beta_L = 1$, included as a reference for the discussion in Appendix B, we have divided the central values (but not the error bars) by a factor 10.

$a^3 \kappa_{\text{latt}}(\omega)$ at various β_L , together with a comparison with the free theory result. Noting that on the 4-dimensional lattice, $\beta = N_\tau a_\tau$, where N_τ , a_τ are the number of lattice points and the lattice spacing in the time direction, respectively, and naively enforcing the replacement of the classical limit of the Bose-Einstein distribution function, T/ω , by the corresponding quantum mechanical expression, $1/2 + n_B(\omega)$, we can expect $\kappa_{\text{cont}}(\omega)$ to behave as

$$\kappa_{\text{cont}}(\omega) \simeq \frac{\omega a_\tau N_\tau}{2} \coth\left(\frac{\omega a_\tau N_\tau}{2}\right) \kappa_{\text{latt}}(\omega). \quad (4.5)$$

In particular, for $\omega \ll T$, $\kappa_{\text{cont}}(\omega)$ should be completely flat just like $\kappa_{\text{latt}}(\omega)$; moreover, in general, $\kappa_{\text{cont}}(\omega)$ should show no peaks other than at $\omega \sim (1.5 - 3.0)/a$, where a is the spatial lattice spacing. We consider these qualitative features to be relatively robust, and they can in any case serve as crosschecks on particular practical inversions of Eq. (4.4).

Finally, we remark that the corresponding spectral functions computed for $\mathcal{N} = 4$ Super-Yang-Mills theory at infinite 't Hooft coupling in continuum show an analogous smooth behavior at small frequencies, taken over by ultraviolet physics at $\omega \sim T$ [4, 37].

5. Summary and Outlook

The purpose of this paper has been to make use of classical lattice gauge theory, in order to gain insights on the dynamics of QCD in the temperature range accessible to current and near-

future heavy ion collision experiments. We have stressed, in particular, that classical lattice gauge theory is a multiscale system just like QCD; unlike QCD, however, it easily lends itself to non-perturbative simulations of real-time observables, in both the weak-coupling and strong-coupling regimes. Thereby a semi-analytic understanding can be obtained of many interesting observables, without changing the number of color degrees of freedom or introducing unphysical infrared fields.

More specifically, we have elaborated on the heavy quark momentum diffusion coefficient, denoted by κ , which determines the heavy quark thermalization rate through linear response relations. This quantity belongs to the general class of observables which are “dominantly” influenced by momenta around the Debye scale, $p \sim gT$. We have shown explicitly through a weak-coupling analysis that while the physics of the classical lattice gauge theory differs from that in QCD on the quantitative level, by effects of up to 50%, the qualitative features of the dynamics do remain intact.

Proceeding from weak coupling towards intermediate coupling, we have furthermore shown that the leading-order weak-coupling expression, and even the larger next-to-leading order expression, *underestimate* the non-perturbative result. Given the close analogy with QCD, the same statement should be true on that side. This seems to give realistic hopes that a future quantitative determination of κ through 4-dimensional lattice Monte Carlo simulations will reveal a large thermalization rate, which might help to explain the surprisingly rapid thermalization that has been observed at RHIC experiments [35].

Finally, with regard to Monte Carlo simulations, we have explored the general structure of the spectral function corresponding to the Euclidean electric field correlator that can be used for determining the thermalization rate [22]. We find that apart from a single peak at the scale of the spatial lattice spacing, the spectral function has little structure, both at weak and at intermediate coupling. This should be an encouraging message with respect to the analytic continuation needed in the analysis of the Monte Carlo simulations.

Acknowledgments

ML and GDM thank Simon Caron-Huot for valuable discussions. The work of GDM was supported in part by the Natural Sciences and Engineering Research Council of Canada, and by the Alexander von Humboldt Foundation through an F. W. Bessel award.

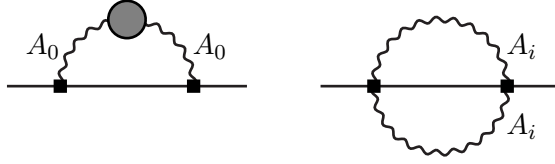


Figure 6: The diagrams contributing to κ_{latt} in Coulomb gauge. The straight lines represent temporal Wilson lines, the closed squares electric fields, and the grey bubble the gauge field self-energy.

Appendix A. Weak-coupling regime in classical lattice gauge theory

We give in this appendix some details concerning the computation of the constant accompanying the logarithm in the leading-order weak-coupling result, Eq. (3.7) (or Eq. (3.13)).

In the “standard” implementation [14] of classical lattice gauge theory, where time is continuous and Minkowskian, the electric field strength has the form

$$aE_i(x) = -\frac{i}{g}[\partial_t U_i(x)]U_i^\dagger(x) + A_0(x) - U_i(x)A_0(x + a\hat{i})U_i^\dagger(x). \quad (\text{A.1})$$

Here U_i are the spatial link matrices. For a perturbative computation we write $U_i = \exp(iagA_i^b T^b)$, where T^b are Hermitean and assumed normalized as $\text{Tr}[T^b T^c] = \delta^{bc}/2$. As usual [38], Fourier representations of the spatial variables are most conveniently chosen as $A_i^b(x) = \int_K A_i^b(K) e^{iK \cdot (x + a\hat{i}/2)}$. Furthermore a gauge needs to be fixed; like in the continuum computation [2], it is convenient to choose a Coulomb gauge so the propagator splits into a transverse spatial part and an A_0 field propagator which has no on-shell spectral weight. In this gauge the result emerges from two graphs, depicted in Fig. 6: the A_0 self-energy diagram, mediated by the vertex

$$A_0^a(P) A_i^b(Q) A_j^c(R) \delta(P + Q + R) \frac{ig}{2} f^{abc} \delta_{ij} \cos(ap_i/2)(R_0 - Q_0), \quad (\text{A.2})$$

plus from one additional graph, namely the bubble diagram sourced by the second term in the expansion of the first term of Eq. (A.1),

$$aE_i(x) = \dots + \frac{1}{2} a^2 g T^b f^{bcd} [\partial_t A_i^c(x)] A_i^d(x) + \dots \quad (\text{A.3})$$

The final result can be written as

$$\begin{aligned} \kappa_{\text{latt}} = & \frac{4\pi g^4 T^2 C_F C_A}{3} \int_{-\pi/a}^{\pi/a} \frac{d^3 \mathbf{p}}{(2\pi)^3} \frac{\tilde{p}^2}{(\tilde{p}^2 + m_D^2)^2} \int_{-\pi/a}^{\pi/a} \frac{d^3 \mathbf{q}}{(2\pi)^3} \frac{\delta((\widetilde{p-q})^2 - \tilde{q}^2)}{\tilde{q}} \\ & \times \left\{ 2 - \frac{\tilde{p}^2}{\tilde{q}^2} + \frac{\tilde{p}^4}{4\tilde{q}^4} + \frac{a^2}{4} \sum_{i=1}^3 \left[\frac{\tilde{p}_i^2 \tilde{q}_i^2 + \tilde{p}_i^2 (\widetilde{p_i - q_i})^2}{\tilde{q}^2} + \frac{\tilde{p}^2 \tilde{q}_i^2 (\widetilde{p_i - q_i})^2}{\tilde{q}^4} \right] \right\}, \quad (\text{A.4}) \end{aligned}$$

where the limit $m_D \ll 1/a$ is assumed.

For the numerical evaluation of Eq. (A.4), one can for instance integrate explicitly over one of the momentum components, to remove the δ -function, and carry out the remaining five-dimensional integral numerically, simplifying the range by making use of various symmetries. More refined strategies are certainly possible but not necessary if only a few digits are needed.

Appendix B. Strong-coupling regime in classical lattice gauge theory

Figure 2 shows that, in the limit $\beta_L \rightarrow 0$, the electric field autocorrelator diverges as $\beta_L^{-5/2}$, while Fig. 5 shows that the frequency spectrum for $\kappa_{\text{latt}}(\omega)$ becomes tightly peaked at small frequencies. What is going on in this regime, and could it have anything to do with QCD? Here we show that the answer to the latter question is almost certainly negative.

To do so we need to discuss a few features of the numerical simulation, which we have otherwise left to the references. Fixing to the temporal gauge, which is convenient because the temporal Wilson lines in the definition, Eq. (1.1), are identity operators, the continuum Yang-Mills theory is described by gauge fields $A_i(\mathbf{x}, t)$ and their canonical momenta, the electric fields $E_i(\mathbf{x}, t)$. On the lattice, the degrees of freedom are the dimensionless electric fields $\mathcal{E}_i = a^2 g E_i + \mathcal{O}(a^3)$ and the gauge links, $U_i(x) = \exp(iagA_i(x))$. We can write $\mathcal{E}_i = \mathcal{E}_i^b T^b$, where T^b are Hermitean generators of the $SU(N_c)$ algebra, normalized as $\text{Tr}[T^b T^c] = \delta^{bc}/2$.

The lattice simulation proceeds by sampling initial configurations with a classical Hamiltonian, and then evolving the configurations in real time through classical equations of motion. The time evolution of the link matrices is

$$a \partial_t U_i(x) = i \mathcal{E}_i(x) U_i(x), \quad (\text{B.1})$$

while for the electric fields it is

$$a \partial_t \mathcal{E}_i^b(x) = 2 \sum_{j \neq i} \text{Im Tr} \left\{ T^b \left[U_j(x) U_i(x + a\hat{j}) U_j^\dagger(x + a\hat{i}) U_i^\dagger(x) + U_j^\dagger(x - a\hat{j}) U_i(x - a\hat{j}) U_j(x + a\hat{i} - a\hat{j}) U_i^\dagger(x) \right] \right\}. \quad (\text{B.2})$$

What is important here is that the spatial link variables are compact. Therefore the size of the time derivative of \mathcal{E}_i^b is bounded. At sufficiently small β_L (strong coupling) the link matrices become essentially random elements of the group, and the typical size of $|a \partial_t \mathcal{E}_i^b|$ saturates. On the other hand, the mean-squared value, $\langle |\mathcal{E}_i^b|^2 \rangle \sim 1/\beta_L$, does not saturate but increases linearly as $1/\beta_L$ is made large.

In this regime, the electric fields feel an essentially random force of fixed mean-squared value, and evolve much like heavy particle velocities in classical Langevin dynamics. The time scale for the link matrices U_i to rotate by an $\mathcal{O}(1)$ angle is $t/a \sim 1/|\mathcal{E}_i^b| \sim \beta_L^{1/2}$. The force on the electric field, Eq. (B.2), involves a product of four links which each rotate independently

at (generically) irrationally related frequencies; the product of four such randomly rotating group elements should show no periodicity or quasi-periodicity. Therefore the coherence time of the random force on \mathcal{E}_i^b is set by the time for a link matrix to rotate by an $\mathcal{O}(1)$ angle, i.e. just $t/a \sim \beta_L^{1/2}$. A random variable \mathcal{E}_i^b with mean squared value $|\mathcal{E}_i^b|^2 \sim \beta_L^{-1}$, experiencing a random force of magnitude ~ 1 with a coherence time $\sim \beta_L^{1/2}$ behaves as $\langle \mathcal{E}_i^b(t) \mathcal{E}_i^b(0) \rangle \sim \langle |\mathcal{E}_i^b|^2 \rangle \exp(-|t|/\tau)$ where $\tau \sim \beta_L^{-3/2}$. Integrating over t and inserting $\langle |\mathcal{E}_i^b|^2 \rangle \sim \beta_L^{-1}$, we conclude that $\kappa \sim \beta_L^{-5/2}$ for $\beta_L \ll 1$. This description also predicts that the support of $\kappa_{\text{latt}}(\omega)$ should become narrow with width $a\omega \sim a/\tau \sim \beta_L^{3/2}$.

However we emphasize that this behavior is an artifact of the electric fields being non-compact while the gauge links U_i are compact. Such a disparity is absent in the quantum theory so the effect is an artifact of the classical lattice discretization. Concretely, we find a different qualitative behavior in the small- β_L regime of the ‘‘improved’’ description (cf. Fig. 4). Therefore we believe that the behavior of κ_{latt} in the small- β_L regime has nothing to do with real QCD.

References

- [1] H. van Hees, V. Greco and R. Rapp, Phys. Rev. C 73 (2006) 034913 [nucl-th/0508055]; H. van Hees, M. Mannarelli, V. Greco and R. Rapp, Phys. Rev. Lett. 100 (2008) 192301 [0709.2884].
- [2] G.D. Moore and D. Teaney, Phys. Rev. C 71 (2005) 064904 [hep-ph/0412346].
- [3] C.P. Herzog, A. Karch, P. Kovtun, C. Kozcaz and L.G. Yaffe, JHEP 07 (2006) 013 [hep-th/0605158]; S.S. Gubser, Phys. Rev. D 74 (2006) 126005 [hep-th/0605182].
- [4] J. Casalderrey-Solana and D. Teaney, Phys. Rev. D 74 (2006) 085012 [hep-ph/0605199].
- [5] K. Kajantie, M. Laine, K. Rummukainen and Y. Schröder, Phys. Rev. D 67 (2003) 105008 [hep-ph/0211321]; A. Vuorinen, Phys. Rev. D 68 (2003) 054017 [hep-ph/0305183]; F. Di Renzo, M. Laine, V. Miccio, Y. Schröder and C. Torrero, JHEP 07 (2006) 026 [hep-ph/0605042].
- [6] A. Hietanen, K. Kajantie, M. Laine, K. Rummukainen and Y. Schröder, Phys. Rev. D 79 (2009) 045018 [0811.4664].
- [7] H. Schulz, Nucl. Phys. B 413 (1994) 353 [hep-ph/9306298].
- [8] S. Caron-Huot and G.D. Moore, Phys. Rev. Lett. 100 (2008) 052301 [0708.4232]; JHEP 02 (2008) 081 [0801.2173].

- [9] M.E. Carrington, A. Gynther and D. Pickering, *Phys. Rev. D* 78 (2008) 045018 [0805.0170].
- [10] S. Caron-Huot, 0811.1603.
- [11] P.M. Chesler and A. Vuorinen, *JHEP* 11 (2006) 037 [hep-ph/0607148]; S. Caron-Huot, P. Kovtun, G.D. Moore, A. Starinets and L.G. Yaffe, *JHEP* 12 (2006) 015 [hep-th/0607237]; S. Caron-Huot, S. Jeon and G.D. Moore, *Phys. Rev. Lett.* 98 (2007) 172303 [hep-ph/0608062]; S.S. Gubser, *Phys. Rev. D* 76 (2007) 126003 [hep-th/0611272].
- [12] J.M. Maldacena, *Adv. Theor. Math. Phys.* 2 (1998) 231 [*Int. J. Theor. Phys.* 38 (1999) 1113] [hep-th/9711200].
- [13] J.B. Kogut and L. Susskind, *Phys. Rev. D* 11 (1975) 395.
- [14] J. Ambjørn, T. Askgaard, H. Porter and M.E. Shaposhnikov, *Nucl. Phys. B* 353 (1991) 346; J. Ambjørn and A. Krasnitz, *Nucl. Phys. B* 506 (1997) 387 [hep-ph/9705380]; G.D. Moore and N. Turok, *Phys. Rev. D* 56 (1997) 6533 [hep-ph/9703266].
- [15] A. Rebhan, P. Romatschke and M. Strickland, *JHEP* 09 (2005) 041 [hep-ph/0505261]; D. Bödeker and K. Rummukainen, *JHEP* 07 (2007) 022 [0705.0180]; P. Arnold and G.D. Moore, *Phys. Rev. D* 76 (2007) 045009 [0706.0490]; J. Berges, D. Gelfand, S. Schefler and D. Sexty, 0812.3859.
- [16] W.H. Tang and J. Smit, *Nucl. Phys. B* 510 (1998) 401 [hep-lat/9702017]; G.D. Moore and N. Turok, *Phys. Rev. D* 55 (1997) 6538 [hep-ph/9608350]; G.D. Moore and K. Rummukainen, *Phys. Rev. D* 63 (2001) 045002 [hep-ph/0009132]; M. Hindmarsh and A. Rajantie, *Phys. Rev. D* 64 (2001) 065016 [hep-ph/0103311].
- [17] J. García-Bellido, M. García Pérez and A. González-Arroyo, *Phys. Rev. D* 69 (2004) 023504 [hep-ph/0304285]; A. Díaz-Gil, J. García-Bellido, M. García Pérez and A. González-Arroyo, *Phys. Rev. Lett.* 100 (2008) 241301 [0712.4263]; A. Rajantie, P.M. Saffin and E.J. Copeland, *Phys. Rev. D* 63 (2001) 123512 [hep-ph/0012097]; E.J. Copeland, D. Lyth, A. Rajantie and M. Trodden, *Phys. Rev. D* 64 (2001) 043506 [hep-ph/0103231]; A. Tranberg and J. Smit, *JHEP* 08 (2006) 012 [hep-ph/0604263]; A. Tranberg, J. Smit and M. Hindmarsh, *JHEP* 01 (2007) 034 [hep-ph/0610096].
- [18] M. Laine, O. Philipsen and M. Tassler, *JHEP* 09 (2007) 066 [0707.2458].
- [19] B. Schenke, M. Strickland, A. Dumitru, Y. Nara and C. Greiner, *Phys. Rev. C* 79 (2009) 034903 [0810.1314].
- [20] D. Bödeker, *Nucl. Phys. B* 486 (1997) 500 [hep-th/9609170].

- [21] G. Aarts and J. Smit, Nucl. Phys. B 511 (1998) 451 [hep-ph/9707342]; W. Buchmüller and A. Jakovác, Nucl. Phys. B 521 (1998) 219 [hep-th/9712093].
- [22] S. Caron-Huot, M. Laine and G.D. Moore, JHEP 04 (2009) 053 [0901.1195].
- [23] B. Svetitsky, Phys. Rev. D 37 (1988) 2484.
- [24] R.D. Pisarski, Phys. Rev. Lett. 63 (1989) 1129; J. Frenkel and J.C. Taylor, Nucl. Phys. B 334 (1990) 199; E. Braaten and R.D. Pisarski, Nucl. Phys. B 337 (1990) 569; J.C. Taylor and S.M.H. Wong, Nucl. Phys. B 346 (1990) 115.
- [25] A.D. Linde, Phys. Lett. B 96 (1980) 289; D.J. Gross, R.D. Pisarski and L.G. Yaffe, Rev. Mod. Phys. 53 (1981) 43.
- [26] D.Y. Grigoriev and V.A. Rubakov, Nucl. Phys. B 299 (1988) 67.
- [27] D. Bödeker, L.D. McLerran and A. Smilga, Phys. Rev. D 52 (1995) 4675 [hep-th/9504123].
- [28] P. Arnold, Phys. Rev. D 55 (1997) 7781 [hep-ph/9701393].
- [29] K. Farakos, K. Kajantie, K. Rummukainen and M. E. Shaposhnikov, Nucl. Phys. B 442 (1995) 317 [hep-lat/9412091].
- [30] M. Laine and Y. Schröder, JHEP 03 (2005) 067 [hep-ph/0503061].
- [31] A.K. Rebhan, Phys. Rev. D 48 (1993) 3967 [hep-ph/9308232]; A. Hart, M. Laine and O. Philipsen, Nucl. Phys. B 586 (2000) 443 [hep-ph/0004060].
- [32] G.D. Moore, Nucl. Phys. B 480 (1996) 657 [hep-ph/9603384].
- [33] G.D. Moore, Nucl. Phys. B 480 (1996) 689 [hep-lat/9605001].
- [34] P. Ginsparg, Nucl. Phys. B 170 (1980) 388; T. Appelquist and R.D. Pisarski, Phys. Rev. D 23 (1981) 2305.
- [35] B.I. Abelev *et al.* [STAR Collaboration], Phys. Rev. Lett. 98 (2007) 192301 [nucl-ex/0607012]; A. Adare *et al.* [PHENIX Collaboration], Phys. Rev. Lett. 98 (2007) 172301 [nucl-ex/0611018].
- [36] F. Karsch, E. Laermann, P. Petreczky and S. Stickan, Phys. Rev. D 68 (2003) 014504 [hep-lat/0303017]; G. Aarts and J.M. Martínez Resco, Nucl. Phys. B 726 (2005) 93 [hep-lat/0507004]; G. Aarts and J. Foley, JHEP 02 (2007) 062 [hep-lat/0612007].
- [37] S.S. Gubser, Nucl. Phys. B 790 (2008) 175 [hep-th/0612143].

- [38] H.J. Rothe, “Lattice gauge theories: An Introduction,” World Sci. Lect. Notes Phys. 74 (2005) 1; S. Capitani, “Lattice perturbation theory,” Phys. Rept. 382 (2003) 113 [hep-lat/0211036].